Desalination and Water Treatment
www.deswater.com
doi: 10.5004/dwt.2021.27520

233 (2021) 81–97
September

Functionalized carbon/alumina/silica nanofibrous membrane: preparation, characterization and heavy metal filtration performance

A. Sepahdar, A. Almasian*, H. Akbari Javar

Department of Pharmaceutical Biomaterials, Faculty of Pharmacy, Tehran University of Medical Sciences, Tehran, Iran, emails: arashalmasi@yahoo.com (A. Almasian), asma.sepahdar@gmail.com (A. Sepahdar), akbarijo@tums.ac.ir/hamidakbari44@yahoo.com (H. Akbari Javar)

Received 2 November 2020; Accepted 9 June 2021

ABSTRACT

In this paper, carbon-based membranes with an extremely high surface area were prepared as a filtration–adsorption membrane for separating Pb^{2+} and Cd^{2+} metal ions from aqueous solutions. High surface area value (1,751.1 m^2 g^{-1}) and unique microscopic structure of nanofibers were obtained with the use of polystyrene (PS) and polyethylene glycol (PEG) as organic and degradable compounds along with aluminum salt and tetraethyl orthosilicate (TEOS) in the polyacrylonitrile (PAN) matrix. The use of aluminum salt and TEOS in the PAN matrix not only influenced the Brunauer–Emmett–Teller value but also enhanced the mechanical properties of membranes. The role of PS, PEG, silica and alumina on surface area and adsorption capacity of heavy metals were evaluated. In order to improve the separation and adsorption ability of the membrane, a functionalization process was performed by triethylenetetramine. The functionalization changed some mechanical properties and hydrophilicity of the membrane resulted in better antifouling property and higher permeability. The antifouling and rejection efficiency of membranes were investigated at two different pH levels. The static adsorption capacity and the rejection efficiency of the functionalized membrane were 450.11, 431.48 mg g^{-1} and 93.25%, 90.11% for Pb and Cd, respectively. The role of mesopores on the adsorption of heavy metals was investigated by adsorption kinetic. The filtration studies revealed that the synthesized membrane has good filtration performance even after 10 regeneration cycles.

Keywords: Carbon nanofibers; Filtration performance; Functionalized nanofibers; Adsorption–filtration membrane

1. Introduction

One of the important worldwide issues affecting human health is the presence of heavy metals in waterways. Increasing the amount of these pollutants is the direct result of the aggravation of industrial activities. Most of these pollutants have toxic, carcinogenic, mutagenic and non-biodegradable nature. Therefore, it is urgent to lower their concentration to an acceptable level.

This problem has been alleviated by using different methods including chemical precipitation, ion exchange, solvent extraction, adsorption, biological processes, electrochemical reduction and membrane separation [1]. Among them, adsorption is known as an effective and economic method for removing heavy metals from wastewater [2]. However, additional procedures are required for separating the adsorbents from the solution which highly increases the operation cost of separation. To overcome

* Corresponding author.

1944-3994/1944-3986 © 2021 Desalination Publications. All rights reserved.

this challenge, the researchers have been developed an adsorption–filtration membrane which is a combination of adsorption and filtration processes. High permeability, high surface porosity, the good pore structure of membranes, hydrophilicity and antifouling nature of membranes are essential parameters for achieving the highest separation efficiency by membranes [3]. Many adsorbents such as oxide minerals, polymeric materials, biosorbents and activated carbon have been used as adsorbents to remove pollutants [4]. Among them, activated carbons have been mostly used to remove a wide variety of organic and inorganic contaminants because of its high surface area, porous structure and the presence of different surface functional groups [5].

Recently, electrospun carbon nanofibers attracted the researcher's attention due to their unique properties such as thermal stability, high surface area, chemical resistance, and micropores opening directly to the outer surface [6]. Polyacrylonitrile (PAN) polymer has been widely used as a precursor to prepare carbon nanofibers because of its low cost and high carbon yield [7,8]. However, it is reported that PAN-derived carbon nanofibers have un-optimized/limited mechanical properties [9]. In this regard, carbon nanomaterials such as carbon nanotubes and graphene are used in combination with PAN matrix to improve the mechanical properties of carbon nanofibers [10]. On the other hand, activated carbon showed poor capacity and affinity for the selective removal of some heavy metals which is related to the lack of selectively specific surface functionalities [11]. In this regard, metal oxides possessing large amounts of terminal hydroxyl groups have been introduced to the carbon nanofibers [11]. Generally, the large pore diameter and high permeability of the electrospun membrane enable it to be a suitable choice for filtering organic pollutants [12]. But, it cannot remove small contaminants like heavy metals efficiently [13]. To overcome this problem, various functional groups including carboxyl, tetrazine, sulfonic, amino, and phosphoric groups have been introduced to the membrane surface [14,15]. The researchers modified the activated carbon with thionyl chloride and ethylenediamine to remove mercury ions from the solution [16]. Also, phenyl-functionalized magnetic activated carbon was prepared for removing the pharmaceutical compound from solutions [17]. The presence of functional groups not only enhances the adsorption capacity of the membrane but also increases the hydrophilicity of the membranes which is an effective way to reduce the surface fouling problem [18].

The total surface area and activity of membranes can be significantly increased by introducing a porous structure to the nanofibers [19]. The porous structure enhances the adsorption ability of adsorbents toward pollutants. Zinc oxide/activated carbon nanofibers with the Brunauer–Emmett–Teller (BET) surface area of 1,404 $m^2\ g^{-1}$ were synthesized by researchers [20]. Porous carbon nanofibers from PAN/SiO_2 precursors with high BET surface area are prepared [6]. Also, electrospun polyacrylonitrile (PAN)-based nanofibers with BET surface area of 450 $m^2\ g^{-1}$ were prepared for the removal of formaldehyde using steam activation that occurred during the carbonization process [21]. The researchers stated that the strength and elastic modulus of PAN-based carbon fiber can tailor by controlling the carbonization and graphitization temperatures [22]. They reported that the tensile strength and elastic modulus reached to its maximum at carbonization temperatures of 1,400°C and 1,700°C, respectively. However, the carbonization procedure at high temperatures requires special equipment for high energy consumption [23]. On the other hand, the creation of porous structure, small fiber diameter, and great specific surface area is the key parameter in the preparation of adsorbents with high adsorption capacity toward pollutants. However, these parameters have adverse effects on the mechanical properties of adsorbents [24]. In this regard, metal oxide nanoparticles such as magnesium oxide (MgO), manganese oxide (MnO_2), zinc oxide (ZnO) and nickel oxide (NiO) have been used to enhance the physicochemical properties of activated carbon nanofibers [25]. In this study, a strong functionalized nanofibrous carbon/alumina/silica membrane was prepared by using tetraethyl orthosilicate (TEOS) as the precursor of silica and aluminum salt in the PAN matrix followed by oxidation and grafting procedure of triethylenetetramine (TETA) on the nanofiber surface. The carbonization process was performed at a relatively low temperature of 700°C. The adsorption capacity and filtration performance of prepared nanofibers toward Pb and Cd ions were evaluated.

2. Experimental

2.1. Materials

Polyacrylonitrile (PAN) copolymer (93.7% acrylonitrile and 6.3% vinyl acetate with M_w = 100.000 g mol^{-1}) was purchased from Isfahan Polyacryl Inc., (Iran). Polystyrene (PS), M_W = 250 kDa, polyethylene glycol (PEG), tetraethyl orthosilicate (TEOS) and N,N-dimethylformamide (DMF) were obtained from Sigma-Aldrich Co. Triethylenetetramine (TETA; 97% purity), aluminum chloride ($AlCl_3$), lead nitrate ($Pb(NO_3)_2$) and cadmium sulfate hydrate ($CdSO_4$, $8H_2O$) were obtained from Merck, Germany.

2.2. Preparation of porous carbon/alumina membrane

PAN (0.65 g) and PS (0.45 g) were dissolved in 10 mL DMF at room temperature. Then, 0.16 g aluminum chloride, 0.16 g PEG and 0.3 g TEOS were added to the solution and it was electrospun under an electrical field range of 16–22 kV, the distance between the tip of needle and collector of 17 cm and the feeding rate of 0.6 mL h^{-1} (hybrid nanofibers, hereafter). The electrospinning apparatus was a Gamma High Voltage Research RR60 power supply and nanofibers were collected onto an aluminum (Al) sheet. The porous carbon/alumina membrane was prepared by placing the hybrid nanofibers in an electrical furnace. Before this step, four nanofiber mats with the dimension of 10 cm^2 × 10 cm^2 were placed on each other and pressed under a weight of 2 kg.

The stabilization step was performed by heating the nanofibers from room temperature to 230°C at a heating rate of 5°C/min with a residence time of 1 h in air. The obtained nanofibers were carbonized at 700°C with a heating rate of 3°C/min. The nanofibers were held at this temperature for 2 h.

2.3. Oxidation process and grafting of TETA on the surface

The oxidation process was conducted by immersing the membrane in 100 mL 5 M HNO_3 solution for 7 h at 40°C followed by washing with deionized water until the aqueous pH > 5. The oxidized membrane (0.5 g) was immersed in a batch containing 10 mL TETA and 30 mL deionized water for 5 min. Then, the membrane was dried at room temperature and placed in a vacuum oven at 125°C for 1 h. After that, the membrane was washed with deionized water and dried. This procedure was repeated 3 times to increase the number of grafted molecules.

2.4. Characterization

The surface morphology of membranes was investigated using a field-emission scanning electron microscope (FE-SEM, Sigma, Zeiss, Germany). The BET surface area and pore size distribution were evaluated using the nitrogen adsorption (Micromeritics Gemini III 2375, USA) and mercury intrusion technique (AutoPore III, Micromeritics Instrument Co., USA), respectively. The elemental analysis was performed on an Elementar Vario EL, USA. An image processor (SXM-196X) was used to determine the average diameter of nanofibers. The measurement of the metal ions concentration was performed by an atomic absorption spectrophotometer (939 Unicam). The porous and core/shell structure of nanofibers was observed by transmission electron microscopy (TEM, JEM-2100, JOEL, Japan) at an accelerating voltage of 200 kV. The mechanical properties of the membranes were evaluated according to ASTM D882-09 using an Instron TE-500 from Farayab, Iran. A CH-1-S thickness meter was used to measure the sample thickness. To achieve this purpose, five random positions were selected to obtain the average thickness. The isoelectric point (IEP) of synthesized nanofibers was determined by the reported method [26]. The swelling ratio was calculated according to the following equation.

$$\text{Swelling ratio}\left(\%\right)=\left(\frac{W_w-W_d}{W_d}\right)\times 100 \tag{1}$$

where W_w and W_d are the membrane weights after swelling for 24 h under wet and dry conditions respectively.

2.5. Filtration studies

The filtration performance of the membrane was evaluated by monitoring the water flux of deionized water (pure water) through the membranes using a dead-end filtration cell. The outer diameter and active filtration area of filtration housing (TAMI Industries, France) were 47 mm and 12.6 cm^2 (40 mm diameter), respectively. The water flux of the different membranes was measured at a pressure of 0.4 MPa at 25°C. 0.4 L of deionized water was passed through the membranes and the filtration time was recorded. The flux, J (L m^{-2} h^{-1}), was calculated as Eq. (2) [27]:

$$J=\frac{Q}{A\Delta t} \tag{2}$$

where Q, A and Δt are the amount of collected pure water (L), the effective membrane area (m^2) and the time of filtration (h), respectively.

Evaluation of the anti-fouling property of membranes was conducted by measuring the flux of water containing bovine serum albumin (BSA) with the concentration of 1 g L^{-1} over 60 min at the pH level of 5.5 and 7.5. The BSA concentrations in the feed and the permeate solutions were measured using a UV-Vis spectrophotometer (Lambda 25, PerkinElmer, USA), at a wavelength of 280 nm. The membranes were washed with pure water for 10 min and the water flux was measured. The flux recovery ratio (FRR) was calculated by the following equation.

$$\text{FRR}\left(\%\right)=\frac{J_2}{J_1}\times 100 \tag{3}$$

where J_2 and J_1 are the water flux of aqueous BSA solution (L m^{-2} h^{-1}) and pure water flux (L m^{-2} h^{-1}), respectively.

Filtration performance toward heavy metals was evaluated by filtering an aqueous solution containing 50 mg L^{-1} heavy metals. The flux was adjusted to 20 L h^{-1}. The concentration of the metal ions in the feed and permeated water was evaluated using atomic absorption spectrophotometer.

The rejection efficiency (R%) of the membranes was calculated as:

$$R\%=\left(1-\frac{C_2}{C_1}\right)\times 100 \tag{4}$$

where C_2 (mg mL^{-1}) and C_1 (mg mL^{-1}) are concentrations of metal ions in the permeate and the feed respectively. All the experiments were done three times and the standard deviation was <5%.

The adsorption capacity of membranes for Pb and Cd ions was determined as Eq. (5).

$$q=\frac{\left(C_0-C_e\right)\times V}{M} \tag{5}$$

where C_0 and C_e are the initial and the equilibrium concentrations of the metal ions in the solution (mg L^{-1}), V is the volume of the solution (L), C is metal ions concentration at $t = t$ and M is the weight of the adsorbent.

3. Result and discussion

3.1. Microscopic characterization

Fig. 1 shows that FE-SEM images of hybrid, carbon/alumina/silica and Functionalized carbon/alumina/silica nanofibers at different magnifications. As can be seen, the hybrid nanofibers presented a uniform morphology with a smooth surface. The average diameter of nanofibers was 288 nm. After the carbonization process, a rigid structure for nanofibers was observed which was due to the degradation of polymeric part and the change of polymeric part (organic) of nanofibers to carbon (inorganic). The rigid structure of inorganic material produced from hybrid templates was reported by researchers [26]. In this case,

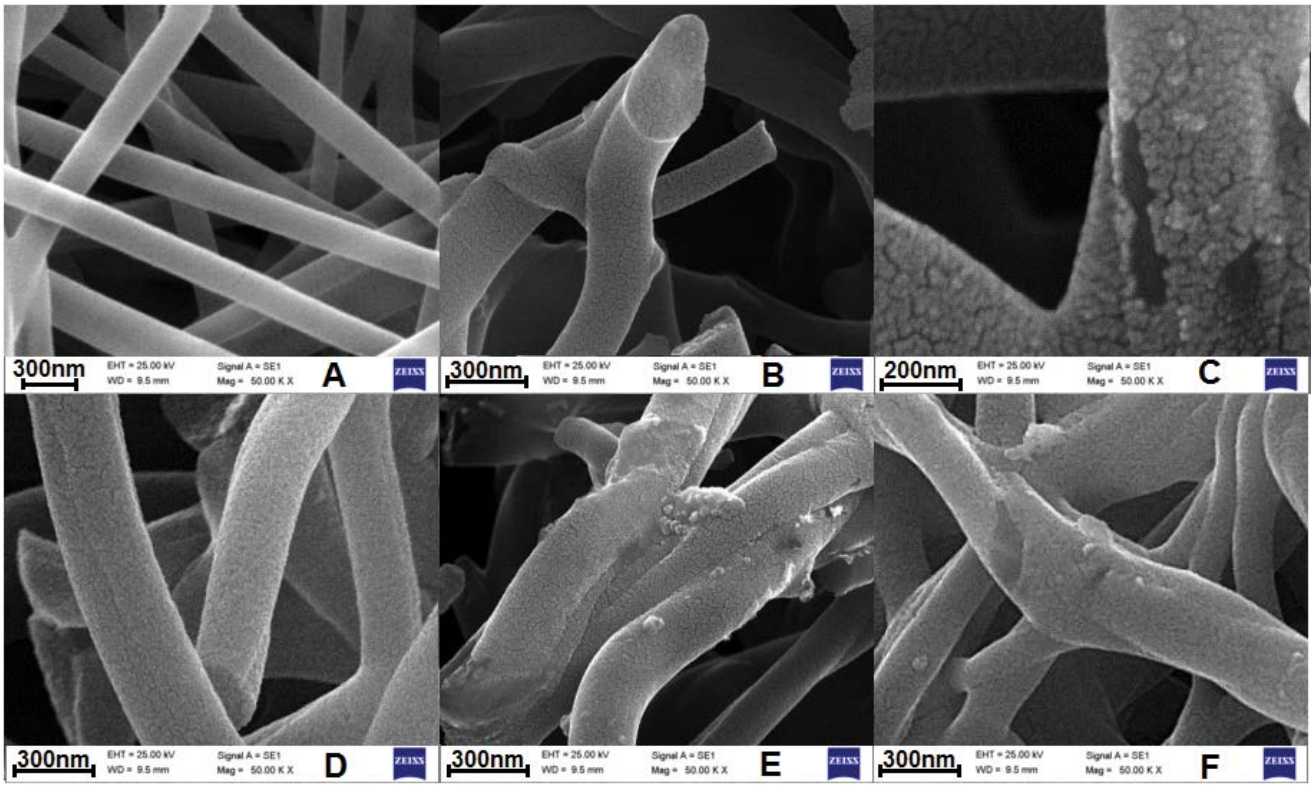

Fig. 1. FE-SEM images of (A) hybrid, (B and C) carbon/alumina/silica, (D) oxidized and (E and F) functionalized nanofibers.

the average diameter of nanofibers was 271.5 nm which was lower than hybrid nanofibers. This was related to the contraction and shrinkage of hybrid nanofibers at high temperatures. From the FE-SEM images, the porous structure of nanofibers was observable. Also, some conglutination of nanofibers especially at their touching points was detected because the addition of TEOS and aluminum salt to the PAN matrix resulted in attaching the adjacent silanol group of silica and Al-O groups together at high temperature (section 3.2). For functionalized nanofibers, there was no significant change in the nanofiber morphology compared to the carbon/alumina/silica sample except for increasing the conglutination of nanofibers. Also, the deposition of a thin layer on the nanofiber surface was detected which can be attributed to grafting the TETA molecules. However, the porous structure was observable even after the deposition of the TETA layer. The average diameter of nanofibers was 275.3 nm. Furthermore, some hollow nanofibers were detected in the images of carbon/alumina/silica and functionalized nanofibers (Fig. 1C and F). According to Fig. 1D, the oxidation process using nitric acid had no effect on the morphology of nanofibers.

TEM images of different nanofibers are shown in Fig. 3. For hybrid nanofibers, the core-shell structure was seen which can be related to the difference between densities of PAN and PS polymers. Previously, it was stated that the mixture of PAN/PS polymers formed a porous carbon structure due to the phase separation phenomenon [28]. In this study, the polymer with lower density (PS) was incorporated in the PAN polymer. The PAN was appeared black (polymer with higher density) and the PS had light color in the images. Also, the core thickness in the core-shell structure was changed along the nanofiber length. It was suggested that core-shell nanofibers resulted in the formation of hollow structures because of the existence of polymeric parts as the core at the whole nanofiber length which can be degraded and formed a hollow structure. Also, the mesoporous structure of nanofibers was detected (Fig. 3E). In TEM images, the presence of some nanoparticles related to the alumina and silica in nanofibers was detected (Fig. 2D). After the functionalization process, a thin layer with a thickness of 5.5 nm was deposited on the nanofiber surface (Fig. 3B).

The surface area of nanofibers was evaluated by BET analysis and the results are shown in Table 1. It was clear that the carbon/alumina/silica nanofibers had an extremely large BET surface area value which was attributed to the porous structure of nanofibers. Also, as mentioned earlier, a hollow structure was observed for some nanofibers which can increase the BET surface area of the sample [29]. Functionalization of nanofibers reduced the BET surface area values from 1751.1 (for carbon/alumina/silica nanofibers) to 1,492 $m^2\ g^{-1}$ due to the filling of some pores existing on the nanofiber surface by TETA molecules. A similar result was reported earlier for functionalizing of Mn_2O_3 nanofibers by acrylic acid [30]. However, the reduction of BET value was not significant indicating that the number of organic molecules grafted on the nanofiber surface was higher than the number of penetrated molecules into the pores. This can be due to the presence of specific sites on the nanofiber surface reacted with TETA and the small size of pores on the surface [31].

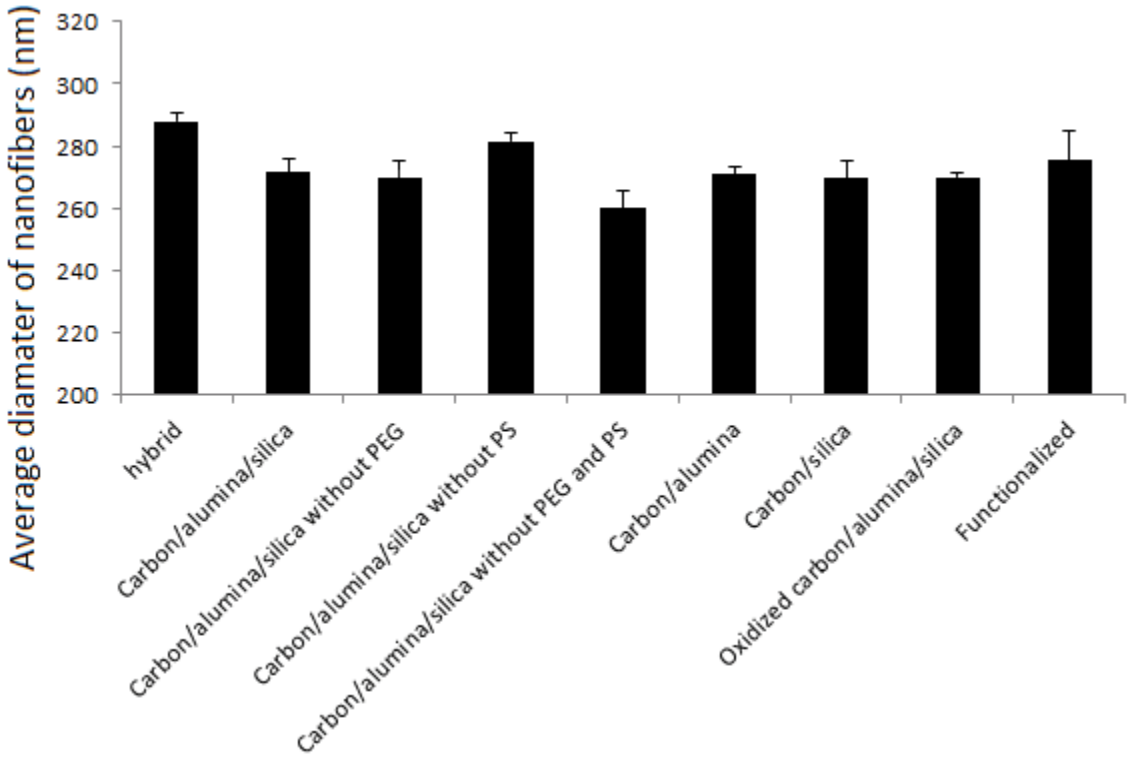

Fig. 2. The average diameter of different nanofiber-based on standard error. The standard deviation values were lower than 1%.

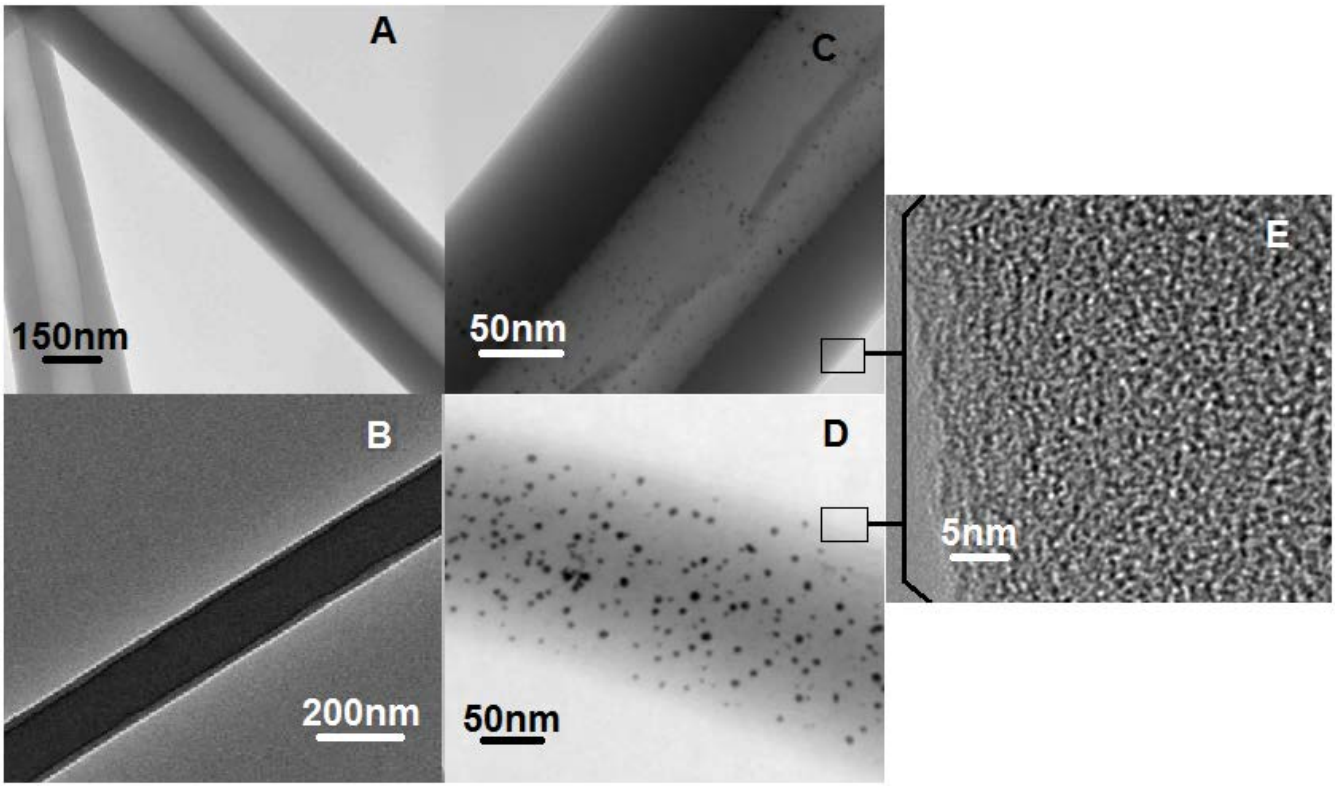

Fig. 3. TEM images of (A) hybrid, (B) functionalized and (C–E) carbon/alumina/silica nanofibers.

Table 1
Result of BET and mercury intrusion analyses for different nanofibers

Method	Based on nitrogen adsorption		Based on mercury intrusion		
Nanofibers	BET ($m^2\ g^{-1}$)	V_m ($cm^3\ g^{-1}$)	V_{total} ($cm^3\ g^{-1}$)	a_p (nm)	Porosity (%)
Hybrid	29.5	8.182	0.270	738.69	69.57
Carbon/alumina/silica	1751.1	507.896	0.252	729.55	68.11
Carbon/alumina/silica without PEG	968.8	254.112	–	–	
Carbon/alumina/silica without PS	787.2	202.361	–	–	
Carbon/alumina/silica without PEG and PS	208	60.588	–	–	
Carbon/alumina	990.7	301.148	–	–	
Carbon/silica	1,070.5	322.195	–	–	
Functionalized	1,492	456.056	0.302	790.21	71.02

V_m: volume of adsorbed nitrogen on the nanofiber surface;
a_p: mean pore diameter;
V_{total}: total pore volume.

The effect of different components used for preparing the nanofibers on BET surface area was investigated and the results are shown in Table 1. As can be seen, the presence of PS in hybrid nanofibers had the most effective in achieving a high BET surface area value. Slow degradation of PS during the carbonization process caused to generate pores on the nanofiber surface [28]. After PS, PEG played a major role which can be probably due to the generation of water molecules by PEG during the carbonization process. The evaporating of water molecules from the matrix formed a porous structure. Porous carbon nanofibers were prepared by using steam during the heat-treatment process [20]. The use of TEOS as the precursor of silica and aluminum salt also increased the BET value. However, the combination of compounds (PS and PEG) resulted in preparing carbon nanofibers with extremely high BET surface area.

The pore size distribution of samples was investigated by Barrett–Joyner–Halenda (BJH) method and the results are presented in Fig. 4. It was obvious that carbon/alumina/silica and functionalized membranes showed a narrow pore size distribution centered at 2.89 and 2.80 nm, respectively, indicating on the mesoporous structure of samples [32]. The porous carbon nanofibers with an average pore size of 2.62 nm were prepared by researchers [20]. The pore size distribution of functionalized membrane was wider than carbon/alumina/silica which was related to the presence of pores with different sizes due to the deposition of TETA molecules on the nanofiber surface. The pore size distribution of the hybrid sample showed an irregular pattern with no distinct peak in the range of 2–50 nm. The mesoporous structure of carbon-based nanofibers was confirmed by the adsorption/desorption isotherms (Fig. 5). The carbon/alumina/silica and functionalized nanofibers showed a type IV isotherm with a type H_3 hysteresis loop suggesting the mesoporous structure of nanofibers. However, the adsorption/desorption isotherm of hybrid nanofibers showed a type II structure indicated on the non-porous structure of nanofibers.

Since, the pore size and the porosity are important parameters affecting on water flux of the membrane, the pore size distribution and porosity of carbon/alumina/silica and functionalized membranes were investigated by the mercury intrusion method and the result is shown in Fig. 6. As can be seen, the pore size distribution curves of carbon/alumina/silica and functionalized membranes centered at 725 and 783.5 nm, respectively. However, functionalized membrane presented a wider distribution than carbon/alumina/silica membrane which was due to the conglutination of nanofibers together. Also, the mean pore diameter of nanofibers (Table 1) was shifted toward higher values because of increased nanofiber diameter [33]. The porosity of functionalized nanofibers increased from 68.11 (for carbon/alumina/silica nanofibers) to 71.02% by the reason for increased nanofiber diameter.

3.2. Mechanical properties of the membrane

The electrospun membranes usually show weak mechanical properties due to their highly porous structure as well as weak bonding between the nanofibers [24]. Therefore, to investigate the filtration performance, an additional substrate is required [34]. The mechanical properties of different membranes were investigated and the result is shown in Table 2. All the reported data are average values obtained from analyzing three randomly selected membrane specimens. For carbon/alumina/silica without PEG, carbon/alumina/silica without PS and carbon/alumina/silica without PEG and PS, the mechanical properties of membranes were proportional to the BET surface area values. With increasing the BET surface area value the tensile strength was decreased due to higher amounts of pores in the nanofiber structure. The sample prepared without PS and PEG showed the highest tensile strength and tensile module due to its non-hollow and non-porous structure and lower average nanofiber diameter. Higher tensile strength of nanofibers at the lower nanofiber diameter value was reported by researchers [22]. The main effect on mechanical properties was attributed to silica and alumina components. It was found that the presence of silica enhances significantly the tensile strength and module. This can be probably due to the interaction of silica with carbon resulted in increasing the interconnections.

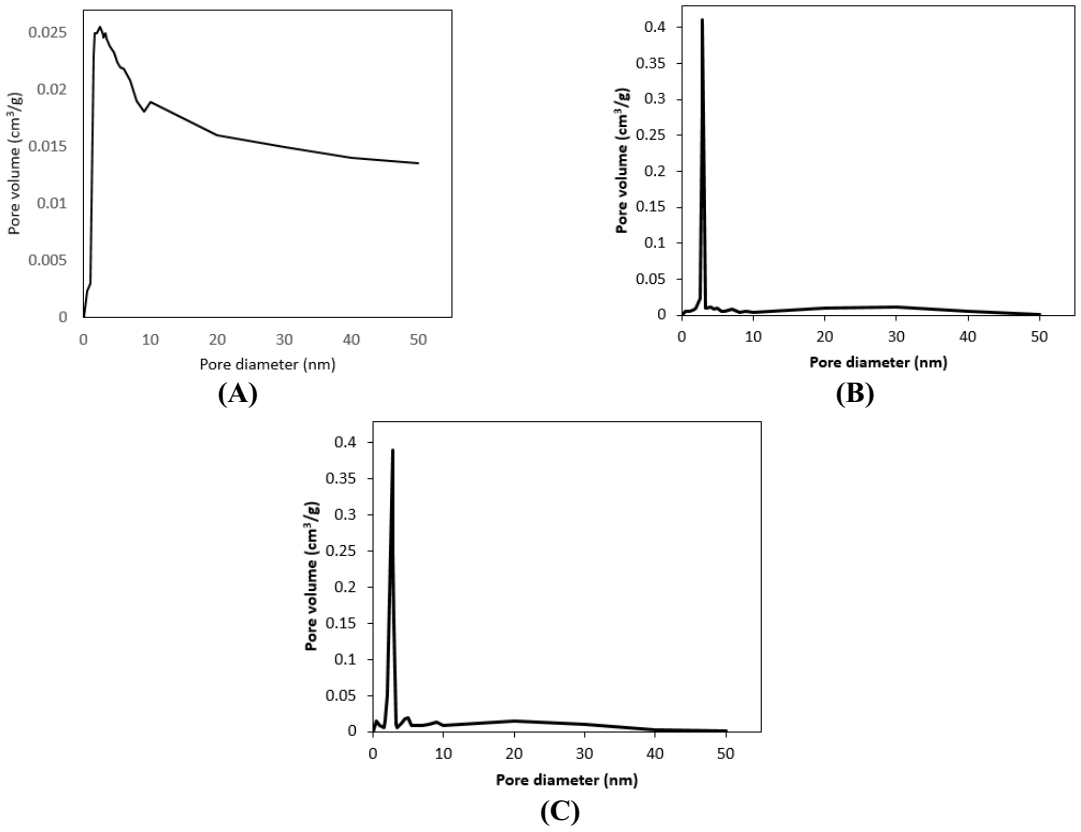

Fig. 4. The pore size distribution (obtained by BJH method) of (A) hybrid, (B) carbon/alumina/silica and (C) functionalized nanofibers.

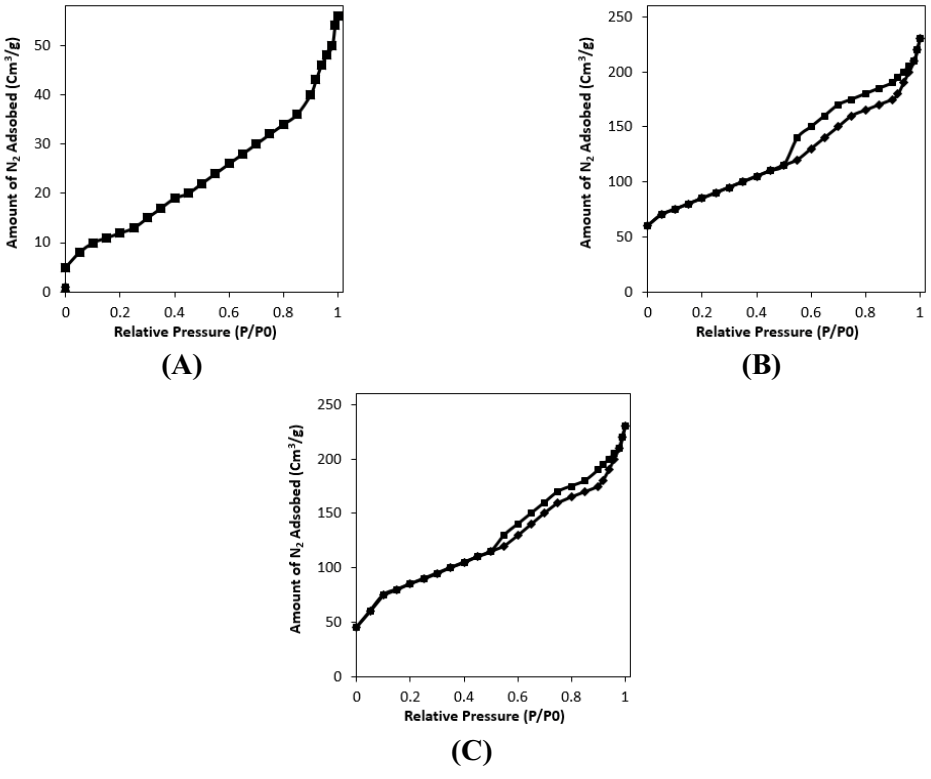

Fig. 5. Nitrogen adsorption/desorption isotherm for (A) hybrid, (B) carbon/alumina/silica and (C) functionalized nanofibers.

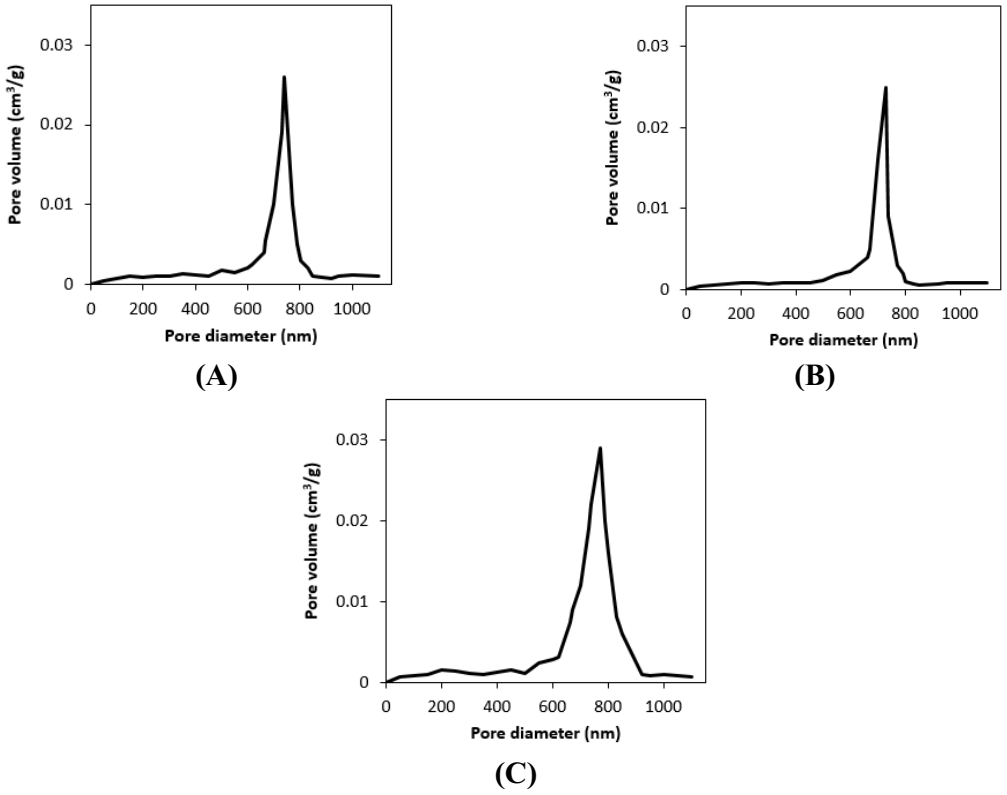

Fig. 6. The pore size distribution (obtained by mercury intrusion method) of (A) hybrid, (B) carbon/alumina/silica and (C) functionalized nanofibers.

Table 2
Mechanical properties of different membranes

Nanofibers	Tensile strength (MPa)	Elongation at break (%)	Tensile module (GPa)	Thickness (μm)	Average diameter (nm)
hybrid	34.21	11	0.31	1.36	288
Carbon/alumina/silica	425.35	1.12	44.60	1.34	271.5
Carbon/alumina/silica without PEG	429.71	1.01	46.12	1.37	270.1
Carbon/alumina/silica without PS	440.84	0.95	46.98	1.35	281.6
Carbon/alumina/silica without PEG and PS	484.02	0.21	49.25	1.34	260
Carbon/alumina	324.66	1.16	32.03	1.37	270.8
Carbon/silica	350.45	1.05	34.14	1.36	269.7
Oxidized carbon/alumina/silica	380.05	1.25	36.13	1.35	270
Functionalized	399.19	1.22	38.65	1.35	275.3

Also, the attachment of silanol and Al-O groups of adjacent nanofibers together during the carbonization process can be regarded as another reason. It was reported that TEOS was responsible for the structural stability of carbon/silica nanofibers [35]. The mechanical properties of carbon nanofibers without silica and alumina could not be investigated by the used instrument because they were crushed easily. It was reported that the surface modification process which increases the hydrophilicity of substrates reduces the mechanical properties of membranes [36]. In this study, the tensile strength of functionalized nanofibers decreased slightly which can be due to the pre-oxidation of nanofibers by nitric acid and the amorphous nature of the deposited layer which had higher elasticity and lower strength compared to the crystalline materials. Although, TETA deposited layer played a crosslinking role on the nanofiber surface it had a negative effect on mechanical behaviors.

3.3. Hydrophilicity of membranes

The hydrophilicity of membranes was determined by water swelling and water contact angle analyses. The

swelling ratio was attributed to the number of hydrophilic sites on the membrane surface and on the membrane morphology [37]. The swelling ratio for carbon/alumina/silica membrane was 3.18% which was increased to 14.25% for functionalized membrane due to the incorporation of amine groups on the nanofiber surface. For the carbon/alumina/silica membrane, the water molecules could be penetrated into the membrane pores. Also, it was stated that the capillary effect in highly porous materials enhances the water absorption property [38].

The wettability of membranes was also investigated by contact angle analysis. The water contact angle for carbon/alumina/silica and functionalized membranes was 131.5° and 21.45°, respectively. The change of hydrophobic nature of carbon/alumina/silica membrane to hydrophilic for functionalized nanofibers was due to the incorporation of TETA molecules onto nanofiber surface. This was also very beneficial to the diffusion and adsorption of ions from the solution to the fiber surface [39].

3.4. Filtration studies

3.4.1. Water flux study

Fig. 7 shows the water flux of membranes at the filtration time of 60 min. The pure water flux for carbon/alumina/silica and the functionalized membrane was 125.66 and 275.23 L m^{-2} h^{-1} at the filtration time of 10 min, respectively. Increasing the water flux value for functionalized membrane was due to the more hydrophilic nature of this membrane. In this study, the hydrophilicity of the membrane was increased due to the incorporation of amine groups on the surface. Also, the average diameter of nanofibers was increased after the functionalization process resulted in higher average pore diameter values. More open pores caused to increase in the water flux values and lowered the resistance of water permeability through the membranes.

3.4.2. Antifouling study

The fouling property of membranes was evaluated by filtration of BSA solution at two pH levels of 5.5 and 7.5 and the results are shown in Fig. 8A. It was found that the water flux for carbon/alumina/silica membrane was decreased from 125.66 (for pure water) to 72.05 L m^{-2} h^{-1} for BSA solution at a pH of 7.5 indicated that BSA was deposited on the surface and pores due to hydrophobic nature of membrane [40]. Also, the flux was decreased during the filtration process due to the fouling of the membrane by BSA molecules. At the pH of 5.5, the water flux showed a higher decline for carbon/alumina/silica membrane because of opposite charge of membrane and BSA resulted in increasing the adsorption of BSA on the membrane surface (the water flux was 51.2 L m^{-2} h^{-1}). For functionalized membrane, the water flux was much higher than carbon/alumina/silica membrane at both pH levels due to the better permeability of the functionalized membrane. A slight decrease from 275.23 (for pure water) to 270 L m^{-2} h^{-1} was observed because of the hydrophilic nature of the membrane which was not favored for adsorption of BSA (pH = 7.5). However, the water flux decreased 3.11% during the filtration process (1 to 60 min). This can be due to the penetration of BSA molecules in the membrane pores. The water flux was 202.6 L m^{-2} h^{-1} when the solution pH was 5.5. The FRR value of carbon/alumina/silica and functionalized membranes were 42.01% and 92.25%, respectively. For hydrophilic membranes, an adsorbed layer of water molecules on the surface hinders the adsorption of protein and other fouling agents. The IEP of carbon/alumina/silica and functionalized membranes were 7.8 and 6.7, respectively. At the pH of 7.5, the surface of the carbon/alumina/silica membrane was relatively neutral and functionalized membrane bore a negative charge. On the other hand, BSA was negatively charged at the pH of 7.5 (IEP of BSA was 4.7–4.9 [41]. Therefore, a self-rejecting layer could be formed on the membrane surface resulted in higher BSA rejection and water flux values. At the pH of 5.5, an electrostatic attraction could occur between the positively charged functionalized membrane and negatively charged BSA molecules which were decreased the water flux value and showed intensified water flux decline. Adsorption of BSA on the membrane surface decreased the water flux due to fouling the pores existing among the nanofibers. The BSA rejection value for carbon/

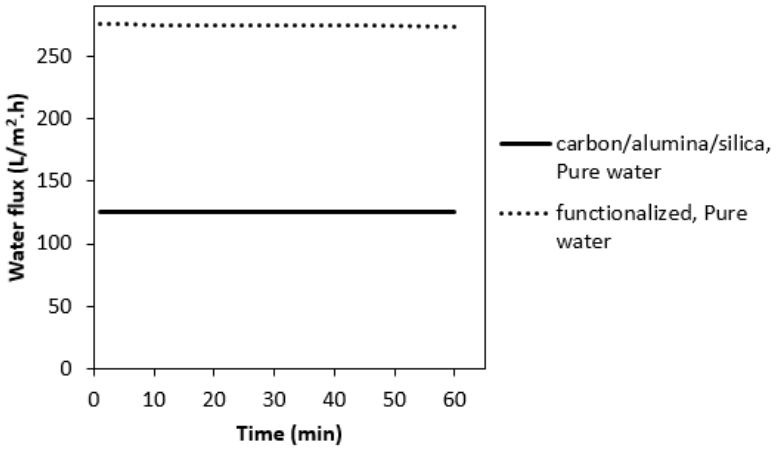

Fig. 7. The water flux of membranes at the filtration time of 60 min.

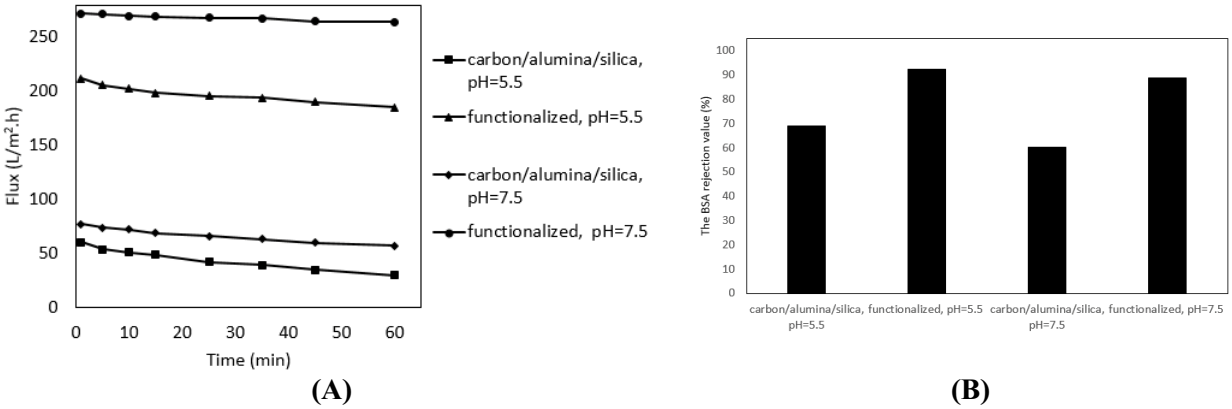

Fig. 8. (A) The fouling property of membranes was evaluated by filtration of BSA solution at two pH levels of 5.5 and 7.5 and (B) The BSA rejection value of carbon/alumina/silica and functionalized membranes at different pH levels.

alumina/silica and functionalized membranes at different pH levels are shown in Fig. 8B. The functionalized membrane had the BSA rejection of 92.46% and 88.91% at the pH of 5.5 and 7.5, respectively. Higher BSA rejection at pH of 5.5 was due to the higher adsorption capacity of the membrane.

3.4.3. Heavy metal ion rejection

The rejection efficiency of membranes for different heavy metals was investigated and the result is shown in Fig. 9. The carbon/alumina/silica membrane showed the rejection efficiency of 48.59% and 44.02% for Pb(II) and Cd(II) ions, respectively (pH = 7.5). For functionalized membranes, the efficiency was increased to 93.25% and 90.11% for Pb(II) and Cd(II) ions, respectively because of incorporating amine groups on the membrane surface which are highly active in formation of complexes with metal ions [42,43]. The presence of amine groups on the surface increases the adsorption capacity toward metal ions because of the incorporation of lone–pair electrons of nitrogen in the vacant orbitals of heavy metal ions and high nucleophilicity of amine groups which is affected on adsorption of metal ions [44,45]. The rejection efficiency of membranes was also evaluated at a pH of 5.5. The results showed that the rejection percentage of carbon/alumina/silica membrane was decreased to 32.05% and 24.52% for Pb and Cd ions, respectively. This can be due to the electrostatic repulsion that occurred between positively charged membrane surface and positively charged metal ions (surface charge of the membrane was dependent on IEP, section 3.4.2). A similar result was observed for functionalized membrane and the rejection efficiency was decreased to 78.1% and 73.54% for Pb and Cd ions, respectively. It was concluded that the electrostatic attraction was the initial driving force of heavy metals binding to the adsorption site of the membrane. The static adsorption capacity of membranes was evaluated at pH = 7.5, membrane dose of 0.01 g, initial metal ion concentration of 100 mg L^{-1}, adsorption time of 60 min and the solution volume of 50 mL. It was found that the carbon/alumina/silica membrane had

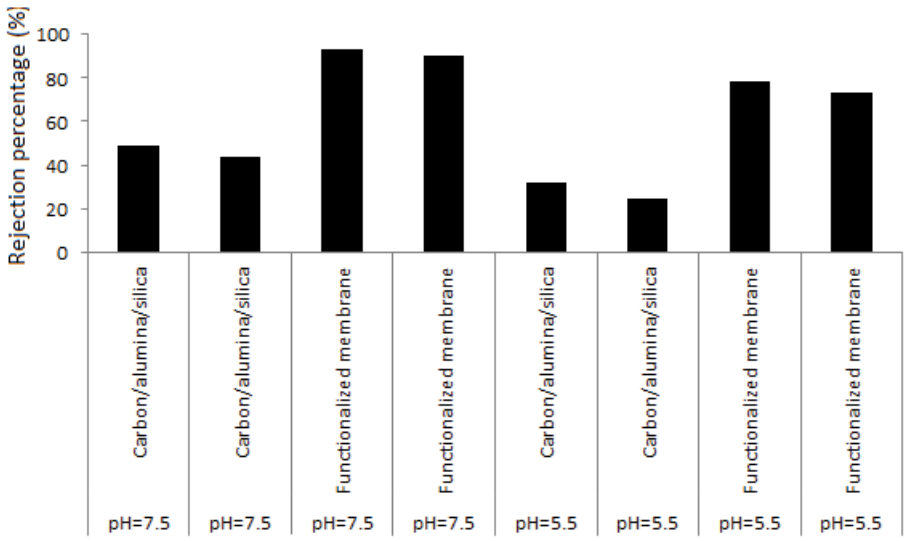

Fig. 9. The rejection percentages of different samples at different pHs.

the adsorption capacity of 230 and 209.25 mg g^{-1} for Pb and Cd ions, respectively. These values were increased to 450.11 and 431.48 mg g^{-1} for functionalized membrane, respectively because of chelating the heavy metals by TETA molecules. Moreover, the metal ions can be encapsulated by TETA chains. Such a result was reported for the adsorbents modified with polyamidoamine (PAMAM) dendrimer [46]. Fig. 10 shows the changes in water flux during the rejection of heavy metals by membranes. As can be seen, the flux of heavy metal-containing water was slightly lower than pure water flux. Also, the flux showed a negligible decrease during the filtration process due to fouling the membrane by heavy metals [34]. However, the shrinkage of TETA chains after the chelation process [47] and the firm structure of membranes that were not deformed mechanically during the filtration process hinder from decreasing the water flux. The water flux of membranes at the filtration of Pb ions was slightly lower than the flux for Cd ions which can be due to the higher adsorption capacity of membranes toward Pb than Cd ions.

As mentioned earlier, the synthesized membranes were highly porous due to the use of PS and PEG. In order to investigate the effect of mesopores on the adsorption efficiency of membranes, the adsorption capacity of membranes produced without the use of PS and PEG was determined as 178.19 and 161.74 mg g^{-1} for Pb and Cd, respectively (carbon/alumina/silica). Also, the capacity was 428.58 and 415.37 mg g^{-1} for functionalized membrane, respectively. It was found that the mesopores on the surface-enhanced the adsorption capability of membranes due to their ability to trap pollutants in their pores. However, the effect of pores on the adsorption capacity of carbon/alumina/silica membrane was more than its effect for functionalized membrane. The adsorption kinetics for adsorption of metal ions by membranes was investigated (section 3.4.4). The effect of the presence of alumina and silica on adsorption property of membranes was investigated and the result is shown in Table 3. It was observed that the presence of silica had a greater influence on the adsorption capacity of carbon/alumina/silica membrane than alumina because the carbon/silica membrane had a higher BET surface area value than carbon/alumina membrane. However, for functionalized membrane, the effect of silica and alumina was lower than un-functionalized membranes confirming that the adsorption of heavy metals was mainly occurred by amine groups.

3.4.4. Adsorption kinetic

The mechanism of solute sorption onto a sorbent can be investigated by employing kinetic models [48]. In this study, pseudo-first-order, pseudo-second-order, and intra-particle diffusion models were used for a better understanding of adsorption behaviors [49]. The non-linearized form of pseudo-first-order equation is expressed as [50]:

$$q_t = q_e\left[1-\exp\left(-k_1\times t\right)\right] \tag{6}$$

where q_e is the amount of adsorbed heavy metals at equilibrium (mg g^{-1}), q_t is the amount of adsorbed heavy metals at t time (mg g^{-1}) and k_1 is the equilibrium rate constant of pseudo-first-order adsorption (min^{-1}).

The non-linear form of the pseudo-second-order kinetic model is as follows [51]:

$$w\, q_t = \frac{k_2\times t\times q_e^2}{\left(1+k_2\times t\times q_e\right)} \tag{7}$$

Table 3
Adsorption capacity value for different prepared membranes

Membrane	Adsorption capacity (mg g^{-1})	
	Pb(II)	Cd(II)
Un-functionalized membrane		
Carbon/alumina/silica	230	209.25
Carbon/alumina	202.58	180.05
Carbon/silica	210.14	187.68
Functionalized membrane		
Carbon/alumina/silica	450.11	431.48
Carbon/alumina	441.87	421.24
Carbon/silica	445.17	427.31

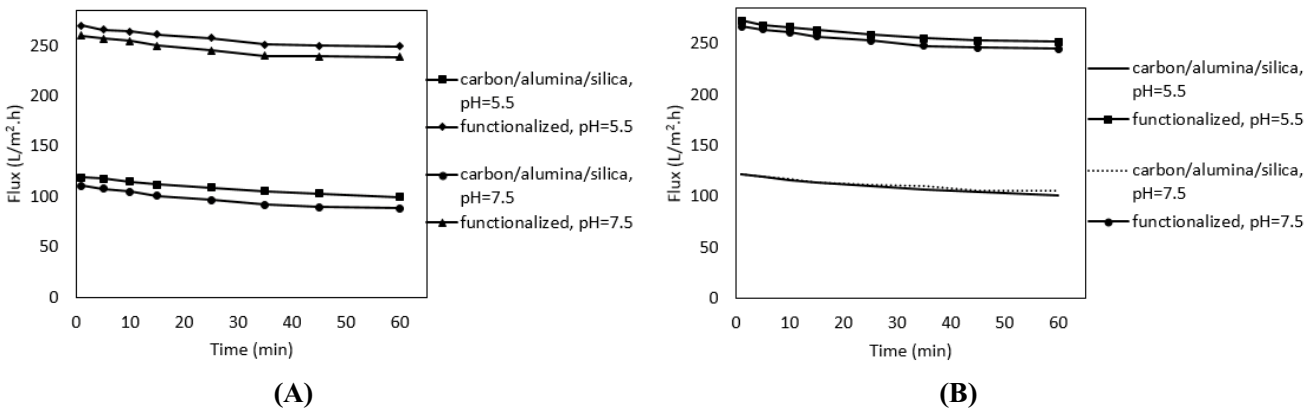

Fig. 10. Water flux of membranes at the rejection of different heavy metals (A) Pb and (B) Cd.

where q_e is the amount of adsorbed heavy metals at equilibrium (mg g^{-1}) and k_2 is the pseudo-second-order equilibrium rate constant (g mg^{-1} min^{-1}).

The intra-particle diffusion model is given as [52]:

$$q_t = k_p t^{\frac{1}{2}} + I \tag{8}$$

where k_p and I are the intra-particle diffusion rate constant and intercept, respectively. The experimental data on the effect of an initial metal ion concentration was fitted to the kinetic models using Data fit version 9.0. In order to optimize the procedure chi-squared error function was used.

The chi-squared test (χ^2):

$$\chi^2 = \sum_{i=1}^{n} \frac{\left(q_{e,\text{calc}} - q_{e,\text{means}}\right)^2}{q_{e,\text{means}}} \tag{9}$$

where n is the number of observations in the experimental data, $q_{e,\text{cal}}$ is equilibrium capacity obtained by calculation from the model (mg g^{-1}) and $q_{e,\text{means}}$ is the equilibrium capacity (mg g^{-1}) from the experimental data.

Table 4 shows the parameters obtained from different kinetic models. It is clear that the carbon/alumina/silica and functionalized membranes followed the pseudo-second-order kinetic model because of higher correlation coefficient and lower error function values. However, the intra-particle diffusion model showed a high correlation coefficient and relatively low error values for both membranes. Since the straight line of intra-particle diffusion models was not passed through the origin indicating that the intra-particle diffusion was not the only rate-controlling step (Fig. 11). It was reported that activated carbon can adsorb various types of pollutants due to the presence of non-localized electrons and reactive groups (including OH, COOH, NH_2 and amide group) in its structure through π-π interactions, hydrogen bonding and charge electrostatic force [53]. Also, they stated that the presence of metal oxide in the activated carbon matrix enhances the adsorption efficiency of activated carbon.

Diffusion within the pore volume (intra-particle diffusion) and diffusion along the surface of the pores (surface diffusion) are involved in the adsorption rate. The adsorption of heavy metals onto the surface of nanofibers

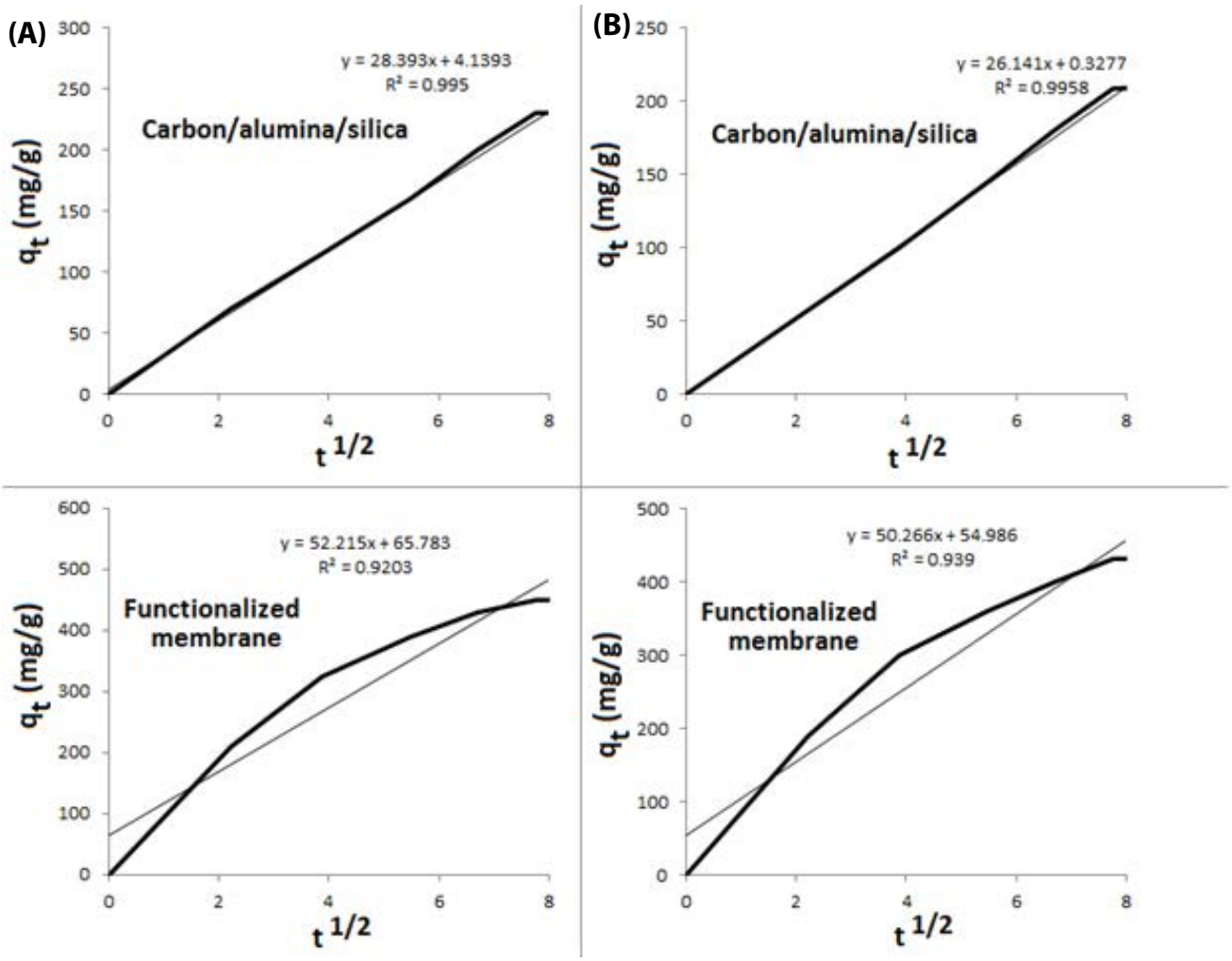

Fig. 11. Intra-particle diffusion model for Pb (A) and Cd (B).

Table 4
The parameters obtained from different kinetic models

Membrane	Carbon/alumina/silica		Functionalized carbon/alumina/silica	
Model	Pseudo-first-order			
Metal ion	Pb(II)	Cd(II)	Pb(II)	Cd(II)
R^2	0.775	0.741	0.805	0.814
$q_{e,cal}$	185.16	180.34	298.66	282.58
k_1	0.128	0.111	0.143	0.131
χ^2	8.086	6.802	6.668	8.822
Model	Pseudo-second-order			
R^2	0.993	0.995	0.999	0.998
$q_{e,cal}$	196.58	187.05	448.25	429.64
$k_2 \times 10^{-2}$	11.25	10.17	3.054	2.485
χ^2	0.868	0.842	0.844	0.886
Model	Intra-particle diffusion			
R^2	0.995	0.994	0.920	0.939
k_p	28.393	26.141	52.215	50.266
I	4.139	0.327	65.78	54.986
χ^2	1.448	1.682	1.156	1.254
Model	Elovich			
R^2	0.685	0.632	0.614	0.599
α	222.58	208.41	335.19	317.51
β	1.11	1.12	2.44	2.58
χ^2	8.889	8.758	8.447	7.896
Model	Boyd			
R^2	0.588	0.541	0.597	0.534
χ^2	0.682	0.698	0.782	0.722

may not be the diffusion control because there is a boundary layer resistance [54]. In this regard, the kinetic data were analyzed by Boyd model represented as Eq. (7) [55].

$$B_t = -0.4977 - \ln\left(1 - F\right) \tag{10}$$

where F is the fraction of solute adsorbed at the time, t (min), and can be calculated from $F = q_t/q_e$. q_e is the amount adsorption capacity at equilibrium (mg g^{-1}). The regression coefficient of the Boyd model is shown in Table 3. The result revealed that although the plot of B_t against time (min) had a high correlation coefficient it had a non-zero intercept indicating that intra-particle diffusion was the rate-controlling step in adsorption of heavy metals by synthesized nanofibers (the figure is not shown).

The kinetic data was also investigated by the Elovich model. Elovich's equation is given as Eq. (8) [56].

$$q_t = \frac{1}{\beta_e}\ln\left(\alpha\beta_e\right) - \frac{1}{\beta_e}\ln t \tag{11}$$

where α and β are constants during any experiment. The constant α is regarded as the initial rate because (dqt/dt) approaches a when q_t approaches α. β_e is related to the extent of activation energy and surface coverage for chemisorptions (g mg^{-1}). The parameters related to the different kinetic models are summarized in Tables 2 and 3. It was found, the R^2 value was low and also the q_e values calculated from the Elovich equation were not agreed with the experimental values. It is reported that the Elovich model has been used for describing the kinetics of the chemisorption process [57].

The linear relationship between the pseudo-rate constant (k_2) and the temperature was used to estimate the activation energy (E_a) of the adsorption [Eq. (9)] [58].

$$\ln k_2 = \ln k_0 - \frac{E_a}{RT} \tag{12}$$

where k_0 is the temperature-independent factor (g mg^{-1} min^{-1}), R is the gas constant (8.314 J mol^{-1} K^{-1}) and T is the solution temperature (K). The result showed that the E_a and k_0 were 50.47 kJ mol^{-1} and 10.14 × 10^4 g mg^{-1} min^{-1} for Pb and 49.84 kJ mol^{-1} and 9.42 × 10^4 g mg^{-1} min^{-1} for Cd ions, respectively indicating on physical adsorption of heavy metals on the nanofiber surface. It is stated that low activation energies (5–50 kJ mol^{-1}) are characteristics for physical adsorption, while higher activation energies (60–800 kJ mol^{-1}) suggest chemical adsorption [59].

3.4.5. Membrane regeneration

The rejection efficiency of heavy metals by different membranes and the water flux after regeneration cycles are shown in Fig. 12. As can be seen, for functionalized membrane, the rejection efficiency and water flux showed a sudden decrease for Pb(II) from 93.25% to 88.29% and 260 to 239.85 L m^{-2} h^{-1}, respectively after the first regeneration cycle. Such a result was observed for Cd(II). These can be due to fouling of mesopores existing on the nanofiber surface and irreversible deformation of the membrane [60]. The decrease of water flux and rejection efficiency with the regeneration cycles was gradual because some of the adsorption sites were lost permanently. Furthermore, the decrease in the rejection efficiency and water flux for carbon/alumina/silica membrane at the first regeneration cycle was much higher than functionalized membrane indicating that the presence of amine groups on the membrane surface-enhanced significantly the filtration performance and regeneration ability of membranes. For carbon/alumina/silica membrane, the rejection efficiency and water flux were 16.1%, 15.89% and 20.42, 22.63 L m^{-2} h^{-1} for Pb and Cd ions, respectively after 10 regeneration cycles. The functionalized membrane showed the rejection efficiency of 86.01% and 81.91% and the water flux of 234.41 and 241.55 L m^{-2} h^{-1} for Pb and Cd ions, respectively after 10 regeneration cycles.

3.4.6. Comparison of membranes with other prepared membranes

In this study, adsorption–filtration membranes were prepared. In this regard, the adsorption capacity of prepared membranes toward heavy metals as compared to some

previously prepared membranes and the result is shown in Table 5. It was clear the functionalized membrane had a much higher adsorption capacity than other previously prepared membranes because of the incorporation of amine groups on the surface and mesoporous structure of the membrane. Also, the adsorption capacity value for carbon/alumina/silica membrane was higher than many prepared adsorbents due to its extremely high surface area and the presence of alumina and silica in the carbon matrix [58,61–63].

Amine-functionalized MCM-41 membrane with the adsorption capacity of 2.8 and 3.7 mg g^{-1} for Cr and Cu, respectively, a maximum water flux of 58.4 L m^{-2} h^{-1} and humic acid rejection of 87.1% was prepared [64]. Chitosan/polyvinyl alcohol/polyethylene glycol/aminated multi-walled carbon nanotubes membrane was prepared for removing Cu ions from solutions. The membrane showed the adsorption capacity of 28.3 mg g^{-1}, water flux of 9 L m^{-2} h^{-1} and rejection efficiency of 95% at an initial metal ion concentration of 10 mg L^{-1} [65]. Polydopamine-polyethersulfone ultrafiltration-adsorption membrane with the static adsorption capacities of 20.23, 17.01 and 10.42 mg g^{-1} for Pb, Cd and Cu ions, respectively was prepared [66]. The membrane showed the rejection efficiency of 92.9% for BSA, maximum water flux of 166 L m^{-2} h^{-1}. Also, the researchers reported that the prepared polyethersulfone/PANI/Fe_3O_4 membrane had the rejection efficiency of 80% toward heavy metal at a low metal concentration of 5 mg L^{-1} and water flux of 52 L m^{-2} h^{-1}. The prepared membrane at the present study showed higher maximum water flux, heavy metal rejection percentages, good antifouling property and higher static adsorption capacity. It was suggested that the prepared membrane can be effectively applied for the removal of Pb and Cd ions from solutions.

4. Conclusion

In this paper, carbon/alumina/silica membrane was prepared through the addition of PS, PEG, aluminum salt and TEOS in PAN polymer followed by stabilization and carbonization processes and it was used for separating heavy metals from solution. The prepared membrane showed a high BET surface area and mesoporous structure. In order to improve the filtration performance, the surface of the membrane was modified with TETA. The modification process enhanced the hydrophilicity of the membrane resulted in higher permeability and better antifouling property. The functionalized membrane showed the lead adsorption capacity of 450.11 mg g^{-1},

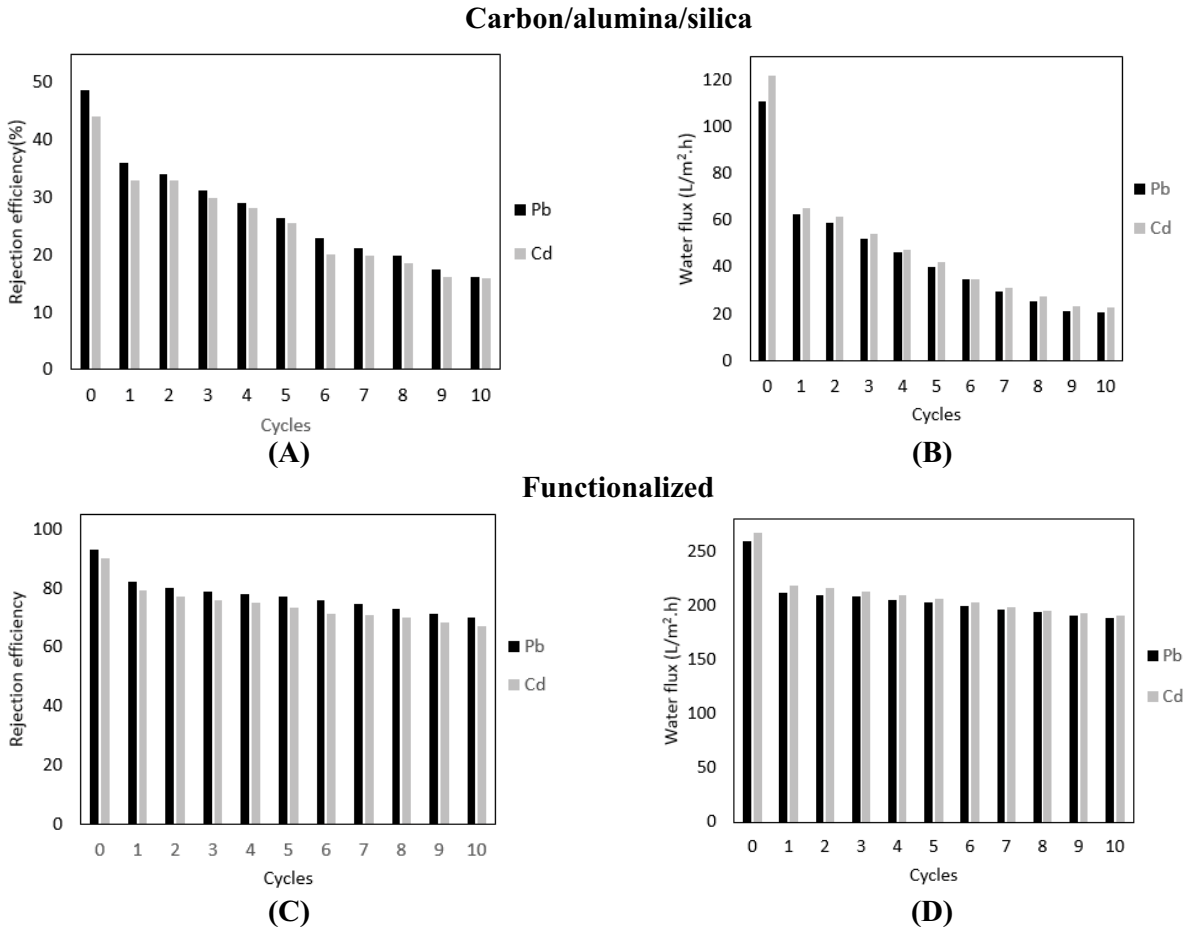

Fig. 12. (A and C) the rejection efficiency of heavy metals by different membranes and (B and D) the water flux after regeneration cycles.

Table 5
The adsorption capacity of prepared membranes toward heavy metals was compared to some previously prepared membranes

Adsorbent	Adsorption capacity (mg g^{-1})	Heavy metal	Ref.
Graphene oxide membranes	72.6	Cu	[61]
	83.8	Cd	
	62.3	Ni	
MnO_2/MWNTs	78.74	Pb	[62]
Magnetite-activated carbon	56.02	Ni	[58]
	58.23	Co	
	63.52	Cd	
Magnetic cellulose-based beads-activated carbon	47.57	Cu	[63]
	37.994	Pb	
	20.80	Zn	
Carbon/alumina/silica	230	Pb	Present study
	209.25	Cd	
Functionalized carbon/alumina/silica	450.11	Pb	Present study
	431.48	Cd	

pure water flux of 275.23 L m^{-2} h^{-1} (at the filtration time of 10 min), Pb rejection of 93.25% and BSA rejection of 92.46% (pH = 5.5) which was much higher than the adsorption capacity (230 mg g^{-1}), pure water flux (125.66 L m^{-2} h^{-1}), heavy metal rejection (48.59%) and BSA rejection (68.88%) (pH = 5.5) for carbon/alumina/silica (un-functionalized) membrane. This was mainly due to the incorporation of amine groups on the membrane surface. The presence of alumina and silica enhanced the mechanical properties and adsorption capacity of membranes. The regeneration studies revealed that the functionalized membrane has high rejection efficiency and water flux even after 10 regeneration cycles. Kinetic studies showed that the adsorption of heavy metal ions from solution had physical nature.

References

[1] M.S. Mansour, M.E. Ossman, H.A. Farag, Removal of Cd(II) ion from waste water by adsorption onto polyaniline coated on sawdust, Desalination, 272 (2011) 301–305.

[2] A. Almasian, M.E. Olya, N.M. Mahmoodi, Synthesis of polyacrylonitrile/polyamidoamine composite nanofibers using electrospinning technique and their dye removal capacity, J. Taiwan Inst. Chem. Eng., 49 (2015) 119–128.

[3] A.K. Nair, A.M. Isloor, R. Kumar, A. Ismail, Antifouling and performance enhancement of polysulfone ultrafiltration membranes using $CaCO_3$ nanoparticles, Desalination, 322 (2013) 69–75.

[4] P.K. Neghlani, M. Rafizadeh, F.A. Taromi, Preparation of aminated-polyacrylonitrile nanofiber membranes for the adsorption of metal ions: comparison with microfibers, J. Hazard. Mater., 186 (2011) 182–189.

[5] M. Karnib, A. Kabbani, H. Holail, Z. Olama, Heavy metals removal using activated carbon, silica and silica activated carbon composite, Energy Procedia, 50 (2014) 113–120.

[6] L. Ji, Z. Lin, A.J. Medford, X. Zhang, Porous carbon nanofibers from electrospun polyacrylonitrile/SiO_2 composites as an energy storage material, Carbon, 47 (2009) 3346–3354.

[7] E.S. Penev, V.I. Artyukhov, B.I. Yakobson, Basic structural units in carbon fibers: atomistic models and tensile behavior, Carbon, 85 (2015) 72–78.

[8] T. Maitra, S. Sharma, A. Srivastava, Y.-K. Cho, M. Madou, A. Sharma, Improved graphitization and electrical conductivity of suspended carbon nanofibers derived from carbon nanotube/polyacrylonitrile composites by directed electrospinning, Carbon, 50 (2012) 1753–1761.

[9] J. Zhu, S. Zhang, L. Wang, D. Jia, M. Xu, Z. Zhao, J. Qiu, L. Jia, Engineering cross-linking by coal-based graphene quantum dots toward tough, flexible, and hydrophobic electrospun carbon nanofiber fabrics, Carbon, 129 (2018) 54–62.

[10] D. Papkov, A.M. Beese, A. Goponenko, Y. Zou, M. Naraghi, H.D. Espinosa, B. Saha, G.C. Schatz, A. Moravsky, R. Loutfy, Extraordinary improvement of the graphitic structure of continuous carbon nanofibers templated with double wall carbon nanotubes, ACS Nano, 7 (2012) 126–142.

[11] L.H. Velazquez-Jimenez, J.A. Arcibar-Orozco, J.R. Rangel-Mendez, Overview of As(V) adsorption on Zr-functionalized activated carbon for aqueous streams remediation, J. Environ. Manage., 212 (2018) 121–130.

[12] M. Anjum, R. Miandad, M. Waqas, F. Gehany, M.A. Barakat, Remediation of wastewater using various nano-materials, Arabian J. Chem., 12 (2019) 4897–4919.

[13] D. Chauhan, S. Afreen, S. Mishra, N. Sankararamakrishnan, Synthesis, characterization and application of zinc augmented aminated PAN nanofibers towards decontamination of chemical and biological contaminants, J. Ind. Eng. Chem., 55 (2017) 50–64.

[14] D. Chauhan, J. Dwivedi, N. Sankararamakrishnan, Facile synthesis of smart biopolymeric nanofibers towards toxic ion removal and disinfection control, RSC Adv., 4 (2014) 54694–54702.

[15] A. Almasian, G. Chizari Fard, M. Parvinzadeh Gashti, M. Mirjalili, Z. Mokhtari Shourijeh, Surface modification of electrospun PAN nanofibers by amine compounds for adsorption of anionic dyes, Desal. Water Treat., 57 (2016) 10333–10348.

[16] J. Zhu, B. Deng, J. Yang, D. Gang, Modifying activated carbon with hybrid ligands for enhancing aqueous mercury removal, Carbon, 47 (2009) 2014–2025.

[17] K.T. Wong, Y. Yoon, S.A. Snyder, M. Jang, Phenyl-functionalized magnetic palm-based powdered activated carbon for the effective removal of selected pharmaceutical and endocrine-disruptive compounds, Chemosphere, 152 (2016) 71–80.

[18] M. Li, Z. Wu, M. Luo, W. Wang, K. Chang, K. Liu, Q. Liu, M. Xia, D. Wang, Highly hydrophilic and anti-fouling cellulose thin film composite membrane based on the hierarchical poly(vinyl alcohol-co-ethylene) nanofiber substrate, Cellulose, 22 (2015) 2717–2727.

[19] C. Kim, Y.I. Jeong, B.T.N. Ngoc, K.S. Yang, M. Kojima, Y.A. Kim, M. Endo, J.W. Lee, Synthesis and characterization of porous

carbon nanofibers with hollow cores through the thermal treatment of electrospun copolymeric nanofiber webs, Small, 3 (2007) 91–95.
[20] C.H. Kim, B.-H. Kim, Zinc oxide/activated carbon nanofiber composites for high-performance supercapacitor electrodes, J. Power Sources, 274 (2015) 512–520.
[21] K.J. Lee, N. Shiratori, G.H. Lee, J. Miyawaki, I. Mochida, S.-H. Yoon, J. Jang, Activated carbon nanofiber produced from electrospun polyacrylonitrile nanofiber as a highly efficient formaldehyde adsorbent, Carbon, 48 (2010) 4248–4255.
[22] S.N. Arshad, M. Naraghi, I. Chasiotis, Strong carbon nanofibers from electrospun polyacrylonitrile, Carbon, 49 (2011) 1710–1719.
[23] D. Papkov, A. Goponenko, O.C. Compton, Z. An, A. Moravsky, X.Z. Li, S.T. Nguyen, Y.A. Dzenis, Improved graphitic structure of continuous carbon nanofibers via graphene oxide templating, Adv. Funct. Mater., 23 (2013) 5763–5770.
[24] C.-L. Pai, M.C. Boyce, G.C. Rutledge, On the importance of fiber curvature to the elastic moduli of electrospun nonwoven fiber meshes, Polymer, 52 (2011) 6126–6133.
[25] F.E.C. Othman, N. Yusof, H. Hasbullah, J. Jaafar, A.F. Ismail, N. Abdullah, N.A.H.M. Nordin, F. Aziz, W.N.W. Salleh, Polyacrylonitrile/magnesium oxide-based activated carbon nanofibers with well-developed microporous structure and their adsorption performance for methane, J. Ind. Eng. Chem., 51 (2017) 281–287.
[26] G.C. Fard, M. Mirjalili, A. Almasian, F. Najafi, PAMAM grafted α-Fe_2O_3 nanofiber: preparation and dye removal ability from binary system, J. Taiwan Inst. Chem. Eng., 80 (2017) 156–167.
[27] L.A. Goetz, B. Jalvo, R. Rosal, A.P. Mathew, Superhydrophilic anti-fouling electrospun cellulose acetate membranes coated with chitin nanocrystals for water filtration, J. Membr. Sci., 510 (2016) 238–248.
[28] S.C. Moon, J.K. Choi, R.J. Farris, Highly porous polyacrylonitrile/polystyrene nanofibers by electrospinning, Fibers Polym., 9 (2008) 276, doi: 10.1007/s12221-008-0044-y.
[29] S.-H. Park, H.-R. Jung, W.-J. Lee, Hollow activated carbon nanofibers prepared by electrospinning as counter electrodes for dye-sensitized solar cells, Electrochim. Acta, 102 (2013) 423–428.
[30] A. Berenjian, L. Maleknia, G.C. Fard, A. Almasian, Mesoporous carboxylated Mn_2O_3 nanofibers: synthesis, characterization and dye removal property, J. Taiwan Inst. Chem. Eng., 86 (2018) 57–72.
[31] G.C. Fard, M. Mirjalili, F. Najafi, Hydroxylated α-Fe_2O_3 nanofiber: optimization of synthesis conditions, anionic dyes adsorption kinetic, isotherm and error analysis, J. Taiwan Inst. Chem. Eng., 70 (2017) 188–199.
[32] Q.-R. Fang, T.A. Makal, M.D. Young, H.-C. Zhou, Recent advances in the study of mesoporous metal-organic frameworks, Comments Inorg. Chem., 31 (2010) 165–195.
[33] A. Almasian, G.C. Fard, M. Mirjalili, M.P. Gashti, Fluorinated-PAN nanofibers: preparation, optimization, characterization and fog harvesting property, J. Ind. Eng. Chem., 62 (2018) 146–155.
[34] K. Yoon, K. Kim, X. Wang, D. Fang, B.S. Hsiao, B. Chu, High flux ultrafiltration membranes based on electrospun nanofibrous PAN scaffolds and chitosan coating, Polymer, 47 (2006) 2434–2441.
[35] C. Ma, J. Sheng, Y. Zhao, R. Wang, H. Zhang, J. Shi, Preparation and comparative study of microporous and mesoporous carbon nanofibers as supercapacitor electrodes, J. Nanosci. Nanotechnol., 18 (2018) 699–704.
[36] X.-Y. Chi, P.-Y. Zhang, X.-J. Guo, Z.-L. Xu, A novel TFC forward osmosis (FO) membrane supported by polyimide (PI) microporous nanofiber membrane, Appl. Surf. Sci., 427 (2018) 1–9.
[37] B. Ganesh, A.M. Isloor, A.F. Ismail, Enhanced hydrophilicity and salt rejection study of graphene oxide-polysulfone mixed matrix membrane, Desalination, 313 (2013) 199–207.
[38] Q. Li, Q. Wei, N. Wu, Y. Cai, W. Gao, Structural characterization and dynamic water adsorption of electrospun polyamide6/montmorillonite nanofibers, J. Appl. Polym. Sci., 107 (2008) 3535–3540.
[39] J. Liu, S. Wang, J. Yang, J. Liao, M. Lu, H. Pan, L. An, $ZnCl_2$ activated electrospun carbon nanofiber for capacitive desalination, Desalination, 344 (2014) 446–453.
[40] Y. Jeyachandran, J. Mielczarski, E. Mielczarski, B. Rai, Efficiency of blocking of non-specific interaction of different proteins by BSA adsorbed on hydrophobic and hydrophilic surfaces, J. Colloid Interface Sci., 341 (2010) 136–142.
[41] L.-P. Zhu, L. Xu, B.-K. Zhu, Y.-X. Feng, Y.-Y. Xu, Preparation and characterization of improved fouling-resistant PPESK ultrafiltration membranes with amphiphilic PPESK-graft-PEG copolymers as additives, J. Membr. Sci., 294 (2007) 196–206.
[42] P. Tahaei, M. Abdouss, M. Edrissi, A. Shoushtari, M. Zargaran, Preparation of chelating fibrous polymer by different diamines and study on their physical and chemical properties, Mater. Sci. Eng. Tech., 39 (2008) 839–844.
[43] A. Almasian, M.E. Olya, N.M. Mahmoodi, Preparation and adsorption behavior of diethylenetriamine/polyacrylonitrile composite nanofibers for a direct dye removal, Fibers Polym., 16 (2015) 1925–1934.
[44] P. Daraei, S.S. Madaeni, N. Ghaemi, E. Salehi, M.A. Khadivi, R. Moradian, B. Astinchap, Novel polyethersulfone nanocomposite membrane prepared by PANI/Fe_3O_4 nanoparticles with enhanced performance for Cu(II) removal from water, J. Membr. Sci., 415 (2012) 250–259.
[45] J.M. Gónzalez-Dominguez, M. Gonzalez, A. Anson-Casaos, A. Diez-Pascual, M. Gomez, M. Martinez, Effect of various aminated single-walled carbon nanotubes on the epoxy cross-linking reactions, J. Phys. Chem. C, 115 (2011) 7238–7248.
[46] M.S. Diallo, W. Arasho, J.H. Johnson Jr., W.A. Goddard 3rd, Dendritic chelating agents. 2. U(VI) binding to poly(amidoamine) and poly(propyleneimine) dendrimers in aqueous solutions, Environ. Sci. Technol., 42 (2008) 1572–1579.
[47] E.N. Zare, M.M. Lakouraj, Biodegradable polyaniline/dextrin conductive nanocomposites: synthesis, characterization, and study of antioxidant activity and sorption of heavy metal ions, Iran. Polym. J., 23 (2014) 257–266.
[48] A. Almasian, N.M. Mahmoodi, M.E. Olya, Tectomer grafted nanofiber: synthesis, characterization and dye removal ability from multicomponent system, J. Ind. Eng. Chem., 32 (2015) 85–98.
[49] L. Ai, H. Yue, J. Jiang, Sacrificial template-directed synthesis of mesoporous manganese oxide architectures with superior performance for organic dye adsorption, Nanoscale, 4 (2012) 5401–5408.
[50] A. Almasian, M. Parvinzadeh Gashti, M.E. Olya, G. Chizari Fard, Poly(acrylic acid)-zeolite nanocomposites for dye removal from single and binary systems, Desal. Water Treat., 57 (2016) 20837–20855.
[51] H.I. Chieng, L.B. Lim, N. Priyantha, Enhancing adsorption capacity of toxic malachite green dye through chemically modified breadnut peel: equilibrium, thermodynamics, kinetics and regeneration studies, Environ. Technol., 36 (2015) 86–97.
[52] X. Xiao, D. Liu, Y. Yan, Z. Wu, Z. Wu, G. Cravotto, Preparation of activated carbon from Xinjiang region coal by microwave activation and its application in naphthalene, phenanthrene, and pyrene adsorption, J. Taiwan Inst. Chem. Eng., 53 (2015) 160–167.
[53] S. Dashamiri, M. Ghaedi, K. Dashtian, M.R. Rahimi, A. Goudarzi, R. Jannesar, Ultrasonic enhancement of the simultaneous removal of quaternary toxic organic dyes by CuO nanoparticles loaded on activated carbon: central composite design, kinetic and isotherm study, Ultrason. Sonochem., 31 (2016) 546–557.
[54] R.-S. Norouzian, M.M. Lakouraj, Preparation and heavy metal ion adsorption behavior of novel supermagnetic nanocomposite based on thiacalix [4] arene and polyaniline: conductivity, isotherm and kinetic study, Synth. Met., 203 (2015) 135–148.
[55] G. Boyd, A. Adamson, L. Myers Jr., The exchange adsorption of ions from aqueous solutions by organic zeolites. II. Kinetics, J. Am. Chem. Soc., 69 (1947) 2836–2848.
[56] R.M. Ali, H.A. Hamad, M.M. Hussein, G.F. Malash, Potential of using green adsorbent of heavy metal removal from aqueous solutions: adsorption kinetics, isotherm, thermodynamic,

mechanism and economic analysis, Ecol. Eng., 91 (2016) 317–332.
[57] M.K. Aroua, C.Y. Yin, F. Lim, W. Kan, W.M.A.W. Daud, Effect of impregnation of activated carbon with chelating polymer on adsorption kinetics of Pb^{2+}, J. Hazard. Mater., 166 (2009) 1526–1529.
[58] A. Azari, B. Kakavandi, R.R. Kalantary, E. Ahmadi, M. Gholami, Z. Torkshavand, M. Azizi, Rapid and efficient magnetically removal of heavy metals by magnetite-activated carbon composite: a statistical design approach, J. Porous Mater., 22 (2015) 1083–1096.
[59] M. Doğan, H. Abak, M. Alkan, Adsorption of methylene blue onto hazelnut shell: kinetics, mechanism and activation parameters, J. Hazard. Mater., 164 (2009) 172–181.
[60] A. Almasian, M. Jalali, G.C. Fard, L. Maleknia, Surfactant grafted PDA-PAN nanofiber: optimization of synthesis, characterization and oil absorption property, Chem. Eng. J., 326 (2017) 1232–1241.
[61] P. Tan, J. Sun, Y. Hu, Z. Fang, Q. Bi, Y. Chen, J. Cheng, Adsorption of Cu^{2+}, Cd^{2+} and Ni^{2+} from aqueous single metal solutions on graphene oxide membranes, J. Hazard. Mater., 297 (2015) 251–260.
[62] H. Wang, A. Zhou, F. Peng, H. Yu, J. Yang, Mechanism study on adsorption of acidified multiwalled carbon nanotubes to Pb(II), J. Colloid Interface Sci., 316 (2007) 277–283.
[63] X. Luo, X. Lei, N. Cai, X. Xie, Y. Xue, F. Yu, Removal of heavy metal ions from water by magnetic cellulose-based beads with embedded chemically modified magnetite nanoparticles and activated carbon, ACS Sustainable Chem. Eng., 4 (2016) 3960–3969.
[64] Y. Bao, X. Yan, W. Du, X. Xie, Z. Pan, J. Zhou, L. Li, Application of amine-functionalized MCM-41 modified ultrafiltration membrane to remove chromium(VI) and copper(II), Chem. Eng. J., 281 (2015) 460–467.
[65] E. Salehi, S. Madaeni, L. Rajabi, A. Derakhshan, S. Daraei, V. Vatanpour, Static and dynamic adsorption of copper ions on chitosan/polyvinyl alcohol thin adsorptive membranes: combined effect of polyethylene glycol and aminated multi-walled carbon nanotubes, Chem. Eng. J., 215 (2013) 791–801.
[66] X. Fang, J. Li, X. Li, S. Pan, X. Zhang, X. Sun, J. Shen, W. Han, L. Wang, Internal pore decoration with polydopamine nanoparticle on polymeric ultrafiltration membrane for enhanced heavy metal removal, Chem. Eng. J., 314 (2017) 38–49.